



Journal Homepage: [-www.journalijar.com](http://www.journalijar.com)

INTERNATIONAL JOURNAL OF ADVANCED RESEARCH (IJAR)

Article DOI: 10.21474/IJAR01/22924
DOI URL: <http://dx.doi.org/10.21474/IJAR01/22924>



RESEARCH ARTICLE

OPTIMIZATION OF ELECTRON AFFINITY IN In_2S_3 BUFFER LAYERS FOR CIGS SOLAR CELLS: A SILVACO ATLAS SIMULATION STUDY

Moussa Toure, Marcel Biagui, Youssou Gning, Aly Toure and Mamadou Lamine Samb

1. Department of Physics and Chemistry, University Iba Der Thiam of Thies, Thies, Senegal.

Manuscript Info

Manuscript History

Received: 04 January 2026

Final Accepted: 08 February 2026

Published: March 2026

Key words:-

CIGS solar cells; In_2S_3 buffer layer; SILVACO ATLAS simulation; Electron affinity; Band alignment; Conduction band offset; Interfacial recombination; Cd-free buffer layer.

Abstract

This study aims to optimize the electron affinity of the indium sulfide (In_2S_3) buffer layer in CIGS solar cells in order to provide a non-toxic alternative to conventional CdS. In_2S_3 exhibits several attractive properties, including a wide optical bandgap (2 – 2.9 eV), high optical transparency, and a tunable electron affinity that enables control of band alignment at the heterojunction interface. A numerical investigation was carried out using the SILVACO ATLAS device simulator to analyze the influence of the buffer-layer electron affinity ($\chi = 4.0 - 4.8$ eV) on the main photovoltaic parameters (J_{SC} , V_{OC} , FF , and η), as well as on the parasitic resistances (R_s and R_{sh}). The simulations were performed under AM1.5G illumination by self-consistently solving Poisson's equation, the carrier continuity equations, and the drift-diffusion transport model. The results indicate that the optimal configuration corresponds to $\chi = 4.0$ eV, yielding a maximum conversion efficiency of 22.96% with a high open-circuit voltage ($V_{OC} = 0.99$ V). This configuration corresponds to a conduction band offset of $\Delta E_C = +0.5$ eV, forming a moderate spike that suppresses interfacial recombination while maintaining efficient electron transport. Increasing the electron affinity significantly improves some resistive parameters (an 83% reduction in R_s and a 14% increase in FF), but simultaneously causes a substantial decrease in the open-circuit voltage (-42%), resulting in an overall efficiency loss of approximately 27%. These results highlight the critical role of band alignment in CIGS/ In_2S_3 solar cells and demonstrate that the open-circuit voltage is the dominant parameter governing device efficiency. The optimal electron affinity window appears to be very narrow ($\Delta\chi < 0.1$ eV), emphasizing the need for precise control of deposition conditions and material stoichiometry.

"© 2026 by the Author(s). Published by IJAR under CC BY 4.0. Unrestricted use allowed with credit to the author."

Introduction:-

Cu (In,Ga)Se₂ (CIGS) solar cells are among the most efficient thin-film photovoltaic technologies, with certified laboratory efficiencies reaching 23.35% [1]. Their device architecture typically consists of a heterojunction formed

between a p-type CIGS absorber and an n-type buffer layer, most commonly cadmium sulfide (CdS). Although CdS plays a crucial role in interface passivation and junction formation, its use raises environmental concerns due to cadmium toxicity and also leads to optical losses in the short-wavelength region [2]. In this context, indium sulfide (In_2S_3) has emerged as a promising Cd-free alternative owing to its wide bandgap (2.0–2.9 eV), high optical transparency, and good chemical stability [3]. Recent studies have shown that the CIGS/ In_2S_3 interface can exhibit a favorable band alignment characterized by an appropriate conduction band offset (CBO), which supports efficient carrier transport [4]. Among the parameters influencing this alignment, the electron affinity (χ) plays a key role because it directly determines the relative position of the conduction bands at the heterointerface. Depending on its value, the CBO may produce either a positive barrier (spike, $\text{CBO} > 0$) or a negative offset (cliff, $\text{CBO} < 0$), which strongly affects interfacial recombination and device performance [5]. In this work, a numerical study based on the SILVACO ATLAS simulator is conducted to investigate the influence of the electron affinity of the In_2S_3 buffer layer ($\chi = 4.0 - 4.8$ eV) on the main photovoltaic parameters (V_{OC} , J_{SC} , FF, η , R_s , and R_{sh}), with the aim of identifying the optimal band alignment configuration for CIGS/ In_2S_3 solar cells. Unlike previous studies that mainly focused on buffer layer doping, this work provides a systematic analysis of electron affinity engineering and its direct impact on band alignment, recombination mechanisms, and photovoltaic performance, highlighting the dominant role of V_{OC} in efficiency optimization.

Methodology:-

The numerical analysis was carried out using the SILVACO ATLAS device simulator, a Technology Computer-Aided Design (TCAD) platform commonly employed for the modeling of semiconductor devices. This tool enables the investigation of the electrical behavior of photovoltaic structures by numerically solving the fundamental transport equations governing charge carriers in semiconductors. In the present study, the simulation framework relies on the self-consistent resolution of Poisson's equation, the carrier continuity equations, and the drift-diffusion transport model, which together describe the electrostatic potential distribution, carrier transport, and generation-recombination processes inside the device [6–8].

Electrostatic potential:-

The electrostatic potential distribution inside the solar cell is determined by Poisson's equation, which relates the spatial variation of the potential ψ to the local charge density within the semiconductor:

$$\text{div}(\epsilon \nabla \psi) = -\rho \quad (1)$$

where ϵ represents the dielectric permittivity of the material and ρ denotes the space charge density.

When free carriers and ionized dopants are taken into account, the space charge density can be expressed as:

$$\text{div}(\nabla \psi) = \Delta \psi = -\frac{q}{\epsilon} [p - n + N_D^+ - N_A^-] \quad (2)$$

where n and p are the electron and hole concentrations, N_D^+ and N_A^- correspond to the densities of ionized donors and acceptors, and q is the elementary charge.

• Carrier conservation

The transport of charge carriers is governed by the continuity equations, which describe the balance between carrier flux, generation, and recombination processes. For electrons and holes, these relations can be written as:

$$\frac{\partial n}{\partial t} = \frac{1}{q} \text{div} \vec{J}_n + G_n - R_n \quad (3)$$

$$\frac{\partial p}{\partial t} = -\frac{1}{q} \text{div} \vec{J}_p + G_p - R_p \quad (4)$$

where \vec{J}_n and \vec{J}_p denote the electron and hole current densities, while $G_{n,p}$ and $R_{n,p}$ represent the carrier generation and recombination rates, respectively.

• Drift-diffusion transport model

Carrier transport in the simulated device is described using the drift-diffusion formalism, which accounts for carrier motion induced by both the electric field and carrier concentration gradients. The current densities for electrons and holes are expressed as:

$$\vec{J}_n = qn\mu_n \vec{E} + qD_n \nabla n \quad (5)$$

$$\vec{J}_p = qp\mu_p \vec{E} - qD_p \nabla p \quad (6)$$

where μ_n and μ_p denote the carrier mobilities, D_n and D_p the diffusion coefficients, and $\vec{E} = -\nabla \psi$ is the electric field derived from the electrostatic potential.

The diffusion coefficients are related to the carrier mobilities through the Einstein relation:

$$D_{n,p} = \frac{\mu_{n,p} k_B T}{q} \quad (7)$$

where k_B is Boltzmann's constant and T is the absolute temperature.

This set of coupled equations provides a comprehensive description of carrier transport and recombination processes in semiconductor devices. Such a modeling framework is widely adopted in TCAD simulations of thin-film photovoltaic devices, including CIGS solar cells, allowing reliable evaluation of the impact of material parameters and interface properties on device performance [8].

Simulated Cell Structure:-

To investigate the influence of the electron affinity of the buffer layer, a typical CIGS thin-film solar cell architecture was considered in the numerical simulations. The complete layer sequence of the device is illustrated in Figure 1.

The simulated structure consists of the following stack:-

SLG / Mo (500 nm) / p-CIGS (2 μm) / n-In₂S₃ (50 nm) / i-ZnO (100 nm) / ZnO:Al (300 nm) / metallic front grid.

This configuration corresponds to the standard architecture widely used in high-efficiency CIGS solar cells. It allows the electrical and optical effects associated with the In₂S₃ buffer layer to be analyzed while maintaining realistic device conditions.

Figure 1 therefore presents the schematic structure of the simulated CIGS/In₂S₃ solar cell.

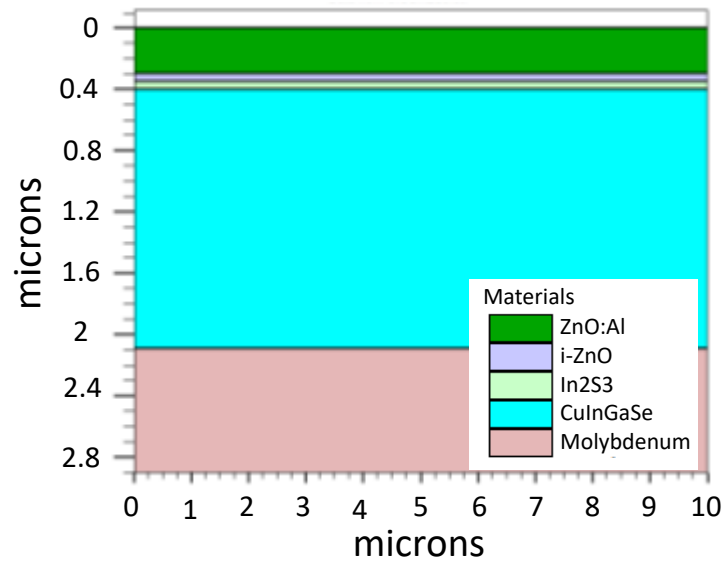


Figure 1: Schematic structure of the CIGS/In₂S₃ solar cell.

As shown in Figure 1, the molybdenum layer provides the back electrical contact, while the p-type CIGS layer acts as the main light-absorbing region. The n-type In₂S₃ layer forms the heterojunction and controls the band alignment at the absorber interface. The intrinsic ZnO layer limits leakage currents, whereas the ZnO:Al layer acts as a transparent conductive oxide ensuring efficient carrier collection at the front contact. With this architecture, any variation in the electrical response of the device can be directly related to changes in the electron affinity of the In₂S₃ buffer layer.

Band Diagram and Conduction Band Offset (CBO):-

The electronic band alignment at the CIGS/In₂S₃ interface plays a crucial role in determining the transport and recombination mechanisms within the device. The energy band configuration associated with this heterojunction is illustrated in Figure 2.

At thermal equilibrium, the band alignment between the two materials is characterized by the conduction band offset (CBO) defined as

$$\text{CBO} = \Delta E_C = E_{C_{\text{In}_2\text{S}_3}} - E_{C_{\text{CIGS}}} \quad (8)$$

Using the definition of electron affinity

$$\chi = E_{\text{vac}} - E_{\text{C}} \quad (9)$$

With E_{vac} : niveau de référence énergétique dans le vide.

The CBO can be expressed as

$$\text{CBO} = \Delta E_{\text{C}} = \chi_{\text{CIGS}} - \chi_{\text{In2S3}} \quad (10)$$

For a typical electron affinity of CIGS, $\chi_{\text{CIGS}} = 4.5$:

- If $\chi_{\text{In2S3}} = 4.0$ eV $\rightarrow \Delta E_{\text{C}} = +0.5$ eV (spike configuration),
- If $\chi_{\text{In2S3}} = 4.8$ eV $\rightarrow \Delta E_{\text{C}} = -0.3$ eV (cliff configuration).

Optimizing the value of χ is therefore essential in order to achieve a favorable band alignment that limits interfacial recombination while maintaining efficient electron extraction [9,10].

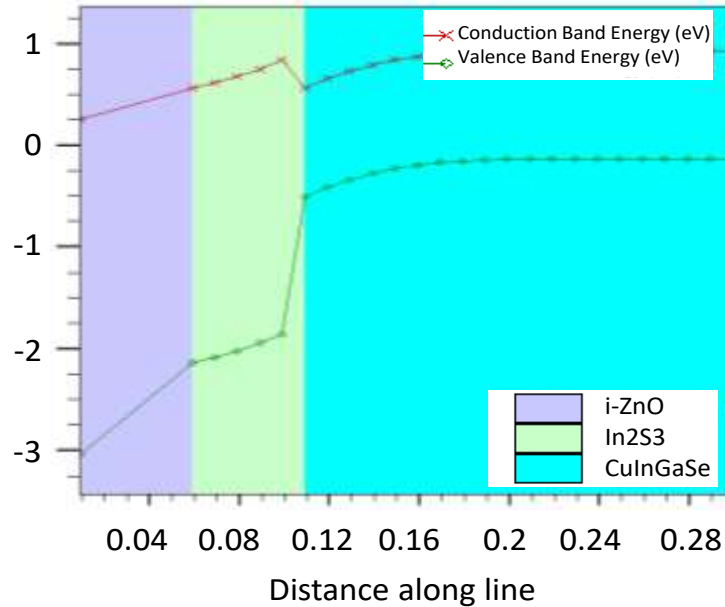


Figure 2: Energy band diagram of the In2S3/CIGS heterojunction at equilibrium.

As illustrated in Figure 2, the conduction band (red curve) and valence band (green curve) correspond to the case $\chi_{\text{CIGS}} = 4.5$ eV and $\chi_{\text{In2S3}} = 4.2$ eV, resulting in a moderate positive offset of approximately $\Delta E_{\text{C}} \approx +0.3$ eV. Such a configuration is generally considered optimal for CIGS heterojunctions since a moderate spike can reduce interfacial recombination by limiting electron backflow toward the absorber while preserving efficient carrier transport. In contrast, a cliff configuration tends to enhance interface recombination and may significantly reduce V_{OC} , whereas an excessively large spike can impede electron extraction and reduce J_{SC} [9,10].

Simulation Parameters:-

The numerical simulations rely on a consistent set of material and device parameters describing the different layers of the solar cell. These parameters include the fundamental electronic properties (bandgap energy, electron affinity, dielectric permittivity), geometrical characteristics (layer thickness), and carrier transport parameters such as mobilities, carrier lifetimes, and effective density of states. All the physical parameters used in the simulations are summarized in Table 1. The numerical simulations conducted in this study are based on a consistent set of physical and electronic parameters accurately describing each layer of the CIGS solar cell. These parameters include fundamental material properties (bandgap energy, electron affinity, dielectric permittivity), geometrical characteristics (layer thickness), as well as carrier transport and recombination quantities (mobilities, carrier lifetimes, effective density of states, and interface trap density).

Table 1: Physical parameters used in the numerical simulations.

Parameters	ZnO:Al	i-ZnO	In ₂ S ₃	CIGS
Optical bandgap E_g (eV)	3.3	3.3	2.7	1.2
Electron affinity χ (eV)	4.45	4.45	4.2	4.5
Relative dielectric permittivity ϵ_r	9	9	13.5	13.6
Thickness (μm)	0,3	0,1	0,05	2
Effective density of states N_C (cm^{-3})	2.2×10^{18}	2.2×10^{18}	2×10^{19}	2.2×10^{18}
Effective density of states N_V (cm^{-3})	1.8×10^{19}	1.8×10^{19}	2×10^{17}	1.8×10^{19}
Donor concentration N_D (cm^{-3})	10^{20}	10^{15}	10^{17}	–
Acceptor concentration N_A (cm^{-3})	–	–	–	5×10^{16}
Electron mobility μ_n ($\text{cm}^2 \cdot \text{V}^{-1} \cdot \text{S}^{-1}$)	100	100	50	100
Hole mobility μ_p ($\text{cm}^2 \cdot \text{V}^{-1} \cdot \text{S}^{-1}$)	25	25	15	25
Electron lifetime τ_n (S)	10^{-10}	10^{-10}	10^{-9}	10^{-7}
Hole lifetime τ_p (S)	10^{-10}	10^{-10}	10^{-9}	10^{-7}
Interface defect density D_{it} ($\text{cm}^{-2} \text{ev}^{-1}$)	–	–	8×10^{11}	–

These values were selected from well-established literature sources and correspond to typical parameters reported for high-performance CIGS solar cells, while ensuring stable numerical convergence within the ATLAS simulation framework [3,9,11]. The interface trap density D_{it} was chosen within realistic ranges to represent partially passivated heterointerfaces, in agreement with experimental observations reported for high-quality CIGS devices [12,13]. In addition, the optical constants of ZnO:Al, i-ZnO and In₂S₃, defined by the complex refractive index $\tilde{n} = n(\lambda) + ik(\lambda)$, were taken from published optical data in order to accurately model photon absorption and carrier generation within the device [14–16].

Extracted Photovoltaic Parameters:-

The electrical behavior of the simulated devices was evaluated from the current–voltage (J–V) characteristics, calculated under standard AM1.5G illumination ($100 \text{ mW} \cdot \text{cm}^{-2}$) at a temperature of 300 K.

From these curves, the main photovoltaic parameters were extracted.

- **Short-Circuit Current Density (J_{SC})**

The short-circuit current density corresponds to the generated current when the applied voltage is zero. It can be expressed as

$$J_{SC} = q \int_0^{\lambda_g} I_0(\lambda) \frac{hc}{\lambda} \text{EQE}(\lambda) d\lambda \quad (11)$$

where $I_0(\lambda)$ is the incident spectral irradiance, h is Planck's constant, c the speed of light in vacuum, $\text{EQE}(\lambda)$ the external quantum efficiency, and q the elementary charge.

- **Open-Circuit Voltage (V_{OC}):**

The open-circuit voltage corresponds to the voltage at which the output current becomes zero:

$$V_{OC} = \frac{nkT}{q} \cdot \ln\left(\frac{J_{SC}}{J_0} + 1\right) \quad (12)$$

where n is the diode ideality factor, k Boltzmann's constant, T the absolute temperature, and J_0 the saturation current density.

- **Fill Factor (FF)**

The fill factor evaluates the quality of the electrical response of the solar cell and is defined by

$$FF = \frac{J_m \times V_m}{J_{SC} \times V_{OC}} \quad (13)$$

where J_m and V_m correspond to the current and voltage at the maximum power point.

- **Conversion Efficiency (η)**

The power conversion efficiency is determined from

$$\eta = \frac{P_m}{P_{in}} = FF \cdot \frac{J_{sc} \times V_{oc}}{P_{in}} \quad (14)$$

where P_m is the maximum output power and P_{in} the incident optical power density [17].

• Series and Shunt Resistances

The parasitic resistances R_s and R_{sh} were extracted from the differential resistance

$$R_{diff} = \left(\frac{dI}{dV} \right)^{-1} \quad (15)$$

evaluated near $V \approx V_{oc}$ for R_s , and near $V \approx 0$ for R_{sh} [18].

This method provides a realistic estimation of resistive losses by accounting simultaneously for transport, recombination, and ohmic effects within the device.

Simulation Campaign:-

The simulation campaign was designed to investigate the influence of the electron affinity of the In_2S_3 buffer layer on the performance of CIGS solar cells. The electron affinity χ was varied from 4.0 to 4.8 eV with a step of 0.1 eV, corresponding to nine distinct configurations. This range allows the exploration of different regimes of conduction band offset (CBO) that control both the band alignment at the CIGS/ In_2S_3 interface and the balance between carrier transport and interfacial recombination mechanisms. All other material parameters, including doping levels, bandgap energies, carrier mobilities, and interface properties, were kept constant throughout the simulations in order to isolate the specific impact of electron affinity on the photovoltaic response of the device.

Results and Discussion:-

Overview of the Results:-

The influence of the electron affinity χ of the In_2S_3 buffer layer on the photovoltaic behavior of the simulated device is summarized in Table 3, which reports the main electrical parameters extracted from the J–V characteristics.

Table 2: Photovoltaic parameters as a function of the electron affinity of In_2S_3 buffer layer.

Electron Affinity χ (eV)	Jsc (mA/cm ²)	Voc (V)	FF (%)	η (%)	Rs ($\Omega \cdot \text{cm}^2$)	Rsh ($\Omega \cdot \text{cm}^2$)
4.0	32.39	0.988	71.8	23.0	6.08	2446
4.1	32.55	0.840	78.1	21.3	1.66	823
4.2	35.07	0.702	72.8	17.9	1.51	179
4.3	36.08	0.588	78.2	16.6	1.20	3776
4.4	36.11	0.571	81.8	16.9	1.04	17112
4.5	36.11	0.571	82.0	16.9	1.03	15872
4.6	36.10	0.571	82.0	16.9	1.03	17689
4.7	36.10	0.571	82.0	16.9	1.03	25920
4.8	36.10	0.572	81.7	16.9	1.07	38439

A clear dependence of the device performance on the value of χ can be observed. In contrast to doping optimization, where carrier transport parameters dominate, the variations reported here are primarily governed by modifications in the band alignment at the CIGS/ In_2S_3 heterointerface, which directly affects the conduction band offset (CBO).

As the electron affinity increases from 4.0 to 4.8 eV, several systematic trends emerge:

- a pronounced decrease in the open-circuit voltage V_{oc} ,
- a moderate increase in the short-circuit current density J_{sc} ,
- a significant reduction in the series resistance R_s ,
- and a strong increase in the shunt resistance R_{sh} at higher χ values.

These trends indicate that the electron affinity plays a key role in determining the electronic behavior of the heterojunction. By modifying the relative position of the conduction bands, χ directly controls the interfacial potential barrier, which in turn governs carrier transport and recombination mechanisms. The results therefore demonstrate that the electron affinity of the buffer layer acts as a critical design parameter in the optimization of CIGS/ In_2S_3 heterojunction solar cells.

Impact on the Power-Voltage (P-V) Characteristic:-

The influence of the electron affinity on the output power characteristics of the device is illustrated in Figure 3, which presents the P-V curves for six representative χ values of the In₂S₃ buffer layer.

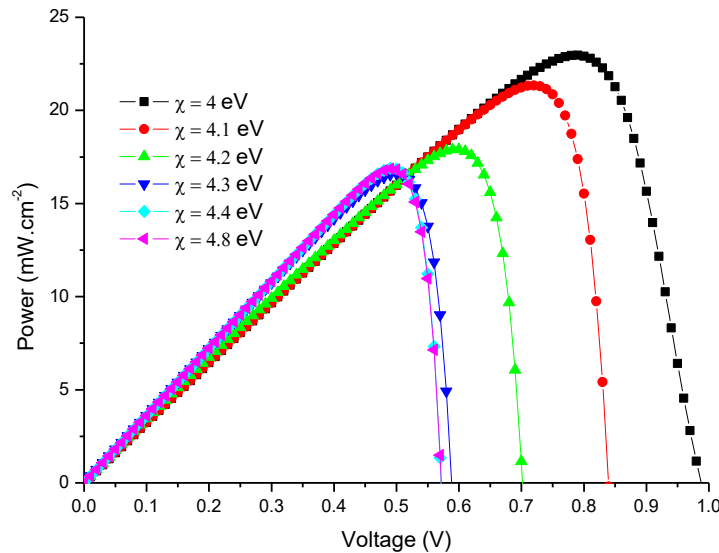


Figure 3: P-V characteristic for different values of electron affinity.

The evolution of the maximum power clearly reveals the strong sensitivity of device performance to the band alignment at the CIGS/In₂S₃ interface. This behavior is primarily governed by the conduction band offset (CBO), a parameter known to strongly influence interfacial recombination and therefore the open-circuit voltage V_{OC} [19]. For $\chi = 4.0$ eV, the device reaches its highest output power, with a maximum power density of approximately $23 \text{ mW} \cdot \text{cm}^{-2}$ obtained at a voltage V_m close to 0.79 V. This operating point corresponds to a very high open-circuit voltage ($V_{OC} \approx 0.99$ V), indicating a low saturation current and limited recombination losses. Such behavior is consistent with a moderate positive conduction band offset (spike configuration), which effectively suppresses electron backflow toward the interface while maintaining efficient carrier extraction [20,21]. The slightly reduced fill factor ($FF \approx 71.8\%$) suggests the presence of ohmic losses, in agreement with the relatively high series resistance ($R_s \approx 6.08 \Omega \cdot \text{cm}^2$) extracted from the J-V characteristics [22]. When the electron affinity increases to $\chi = 4.1$ eV, the maximum power decreases to approximately $21 \text{ mW} \cdot \text{cm}^{-2}$, accompanied by a shift of the maximum power point toward lower voltages ($V_m \approx 0.71$ V). This behavior indicates that even small variations in electron affinity significantly modify the band alignment and the associated recombination dynamics at the heterointerface [19,22]. A further increase to $\chi = 4.2$ eV results in a more pronounced reduction of the maximum power ($P_{max} \approx 18 \text{ mW} \cdot \text{cm}^{-2}$), suggesting that recombination mechanisms or unfavorable interface barriers begin to dominate the device behavior [20,22].

For $\chi \geq 4.3$ eV, the P-V curves exhibit lower power maxima (approximately $16 - 17 \text{ mW} \cdot \text{cm}^{-2}$) but become more rectangular, reflecting a significant increase in the fill factor ($> 82\%$). This improvement is associated with the combined effect of a reduced series resistance and a large shunt resistance. However, these favorable resistive conditions cannot compensate for the strong reduction of the open-circuit voltage ($V_{OC} \approx 0.57$ V), which is typically linked to the transition toward a cliff-type band alignment (negative CBO). In this regime, the absence of a selective barrier enhances interfacial recombination and increases the saturation current density [21–23]. Overall, the results indicate that the efficiency maximum obtained at $\chi = 4.0$ eV results from a delicate balance between carrier transport and recombination. In this device configuration, maintaining a high open-circuit voltage through favorable band alignment proves more critical than minimizing resistive losses alone.

Impact on the Current-Voltage (J-V) Characteristic:-

The influence of the electron affinity of the In₂S₃ buffer layer on the electrical behavior of the device is illustrated in Figure 4, which presents the simulated J-V characteristics under AM1.5G illumination for different χ values.

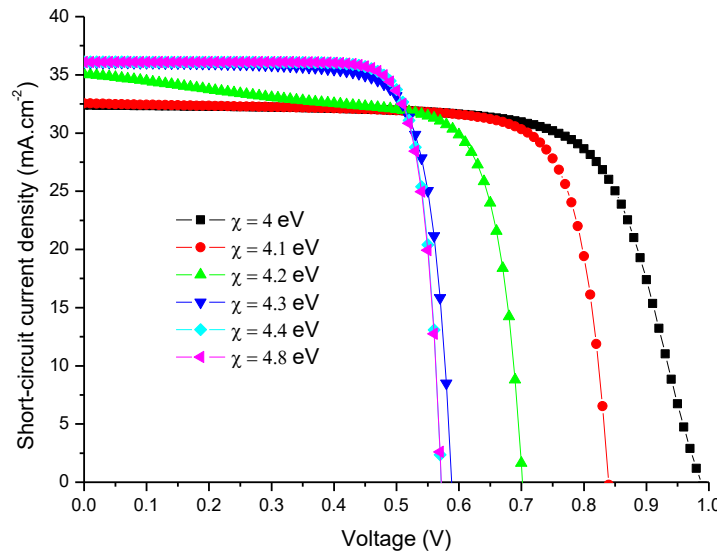


Figure 4: J–V characteristic for different values of electron affinity.

The curves reveal two opposite trends as χ increases: a moderate increase in the short-circuit current density J_{SC} , accompanied by a pronounced reduction in the open-circuit voltage V_{OC} . Such behavior is typical of heterojunction devices where modifications of the conduction band offset (CBO) improve carrier extraction while simultaneously weakening the selectivity of the interface, thereby enhancing recombination and increasing the saturation current [20,21]. For $\chi = 4.0$ eV, the simulated device exhibits a relatively moderate current density ($J_{SC} \approx 32.4 \text{ mA} \cdot \text{cm}^{-2}$) but a very high open-circuit voltage ($V_{OC} \approx 0.99 \text{ V}$). This behavior can be attributed to the presence of a positive CBO (spike configuration) at the CIGS/ In_2S_3 interface. Such a spike acts as an electron-selective barrier that limits electron back-diffusion toward the interface and therefore reduces recombination with holes in the absorber layer [21,23]. However, this barrier can also slightly impede electron extraction, which explains the somewhat lower J_{SC} compared with cases where the interface becomes more transparent to carrier transport [20,22]. When the electron affinity increases beyond $\chi \geq 4.4$ eV, the current density reaches its maximum value ($J_{SC} \approx 36.1 \text{ mA} \cdot \text{cm}^{-2}$), corresponding to an increase of approximately 11.4%. This improvement is consistent with enhanced carrier collection resulting from reduced series resistance and a band alignment progressively approaching a cliff configuration, which facilitates electron transport across the interface.

However, this favorable effect on current is accompanied by a dramatic reduction of the open-circuit voltage ($V_{OC} \approx 0.57 \text{ V}$). In this regime, the absence of a selective barrier allows electrons to accumulate near the heterointerface, where they recombine efficiently with the majority holes present in the CIGS absorber. This process leads to a strong increase in the saturation current density J_0 , which severely limits V_{OC} [21–23]. The transition occurring around $\chi \approx 4.2$ eV therefore marks a change of operating regime in which interfacial recombination progressively dominates the device behavior, even though the resistive parameters may appear favorable [20,22]. Overall, these results confirm that the electron affinity χ_s , through its influence on the CBO, governs the delicate balance between carrier collection and recombination at the CIGS/ In_2S_3 interface. The efficiency maximum obtained for $\chi = 4.0$ eV reflects this compromise: although the spike slightly limits electron extraction, it effectively suppresses interfacial recombination and therefore preserves a high open-circuit voltage.

Influence on the Open-Circuit Voltage V_{OC} :-

The dependence of the open-circuit voltage on the electron affinity χ is presented in Figure 5.

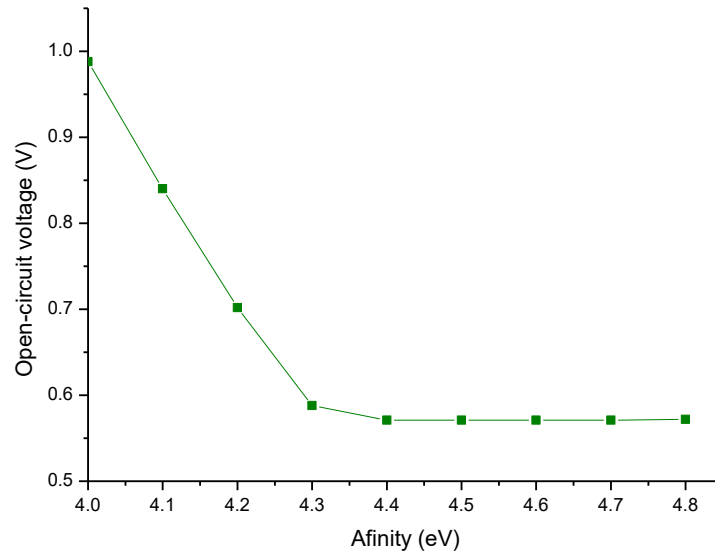


Figure 5: Evolution of the open-circuit voltage as a function of the electron affinity of the In_2S_3 buffer layer

The results show a strong sensitivity of V_{OC} to variations in χ , highlighting the central role of band alignment at the CIGS/ In_2S_3 interface in controlling recombination processes [24,25]. In the first regime, corresponding to χ values between 4.0 and 4.3 eV, the open-circuit voltage decreases rapidly from 0.988 V to 0.588 V. Such a large variation over a relatively narrow χ range illustrates the strong influence of the conduction band offset on the recombination dynamics at the heterojunction, a phenomenon widely reported for CIGS-based solar cells [26,27]. According to the fundamental relationship linking V_{OC} to the saturation current density (see Equation 12), an increase in J_0 inevitably results in a decrease in V_{OC} . The connection between recombination, saturation current, and voltage has been rigorously established through the reciprocity relations and the radiative efficiency limits of photovoltaic devices developed by Rau [22,28]. Consequently, any modification of band alignment that enhances interfacial recombination leads to an exponential increase in J_0 and a corresponding reduction in V_{OC} . For $\chi = 4.0$ eV, the positive conduction band offset ($\Delta E_C = +0.5\text{eV}$) creates a spike that acts as a selective barrier at the heterointerface. This barrier reduces the probability of electron back-diffusion toward the interface and therefore limits electron-hole recombination [25,26]. The resulting decrease in J_0 allows the device to achieve a high open-circuit voltage approaching the theoretical radiative limit [28].

As χ increases, the CBO progressively decreases and eventually becomes negative, corresponding to a cliff configuration. In this regime, electrons can more easily reach the heterointerface where holes are abundant in the p-type absorber, thereby enhancing interfacial recombination processes [24,26,27]. The associated increase in J_0 leads to the observed collapse of V_{OC} , in agreement with the theoretical relationship between recombination and open-circuit voltage [22,28]. These results clearly demonstrate that the electron affinity indirectly controls the open-circuit voltage through its effect on the conduction band offset and the resulting recombination dynamics. Consequently, V_{OC} emerges as the photovoltaic parameter most sensitive to band alignment in CIGS/ In_2S_3 heterojunction solar cells [25,26].

Influence on the Short-Circuit Current Density J_{SC} :-

The variation of the short-circuit current density with the electron affinity of the In_2S_3 buffer layer is illustrated in Figure 6.

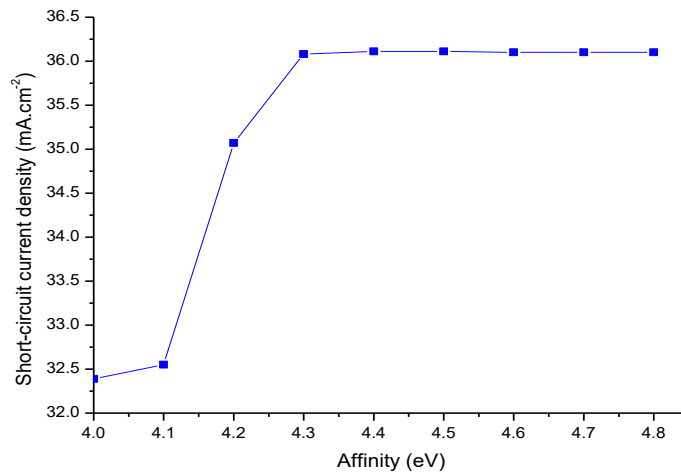


Figure 6: Short-circuit current density profile as a function of electron affinity.

Unlike the open-circuit voltage, which is strongly controlled by recombination mechanisms, the short-circuit current density is primarily determined by carrier collection efficiency and transport conditions within the device [24–29]. As the electron affinity increases from $\chi = 4.0$ to 4.3 eV, J_{SC} rises significantly from 32.4 to 36.1 mA·cm⁻², corresponding to an increase of approximately 11.4%. This improvement can be mainly attributed to the strong reduction in the series resistance, which decreases from 6.08 to 1.20 Ω·cm², thereby facilitating carrier transport and reducing resistive losses. Beyond $\chi = 4.3$ eV, the current density reaches a plateau around 36.1 mA·cm⁻², indicating that the beneficial effect associated with the reduction of R_s has reached its limit. At $\chi = 4.0$ eV, the presence of a positive conduction band offset ($\Delta E_C = +0.5$ eV) forms a spike barrier at the heterointerface. Although this barrier slightly limits electron injection across the interface, it does not significantly impede carrier collection under short-circuit conditions because the internal electric field assists the extraction of photogenerated carriers [25,26].

When χ increases and the conduction band offset approaches zero or becomes negative, the interface becomes more transparent to electron transport, which explains the observed increase in J_{SC} [25,29]. However, this improved carrier injection simultaneously enhances interfacial recombination, which increases the saturation current J_0 and consequently reduces V_{OC} , in accordance with the reciprocity relations established by Rau [28]. As a result, the moderate gain in J_{SC} cannot compensate for the much larger loss in V_{OC} , explaining the overall decrease in efficiency observed at higher χ values.

Influence on the Fill Factor (FF):-

The evolution of the fill factor as a function of electron affinity is presented in Figure 7.

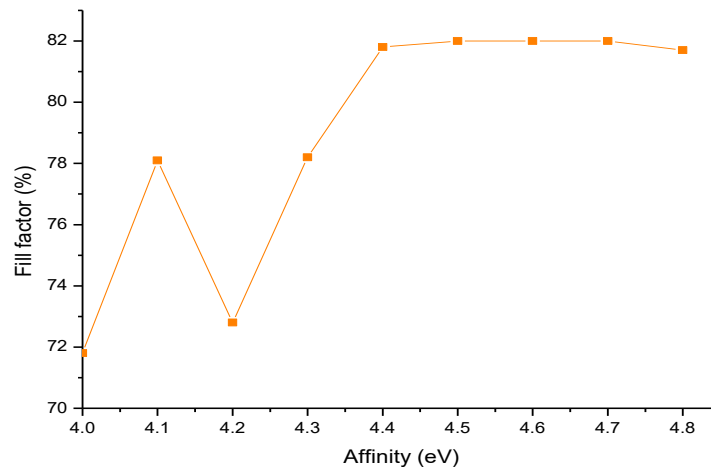


Figure 7: Fill factor profile as a function of electron affinity

The fill factor is mainly influenced by parasitic resistances and recombination mechanisms, which determine the shape and rectangularity of the J–V curves [24,27,29]. For $\chi = 4.0$ eV, the fill factor reaches 71.8%, reflecting the influence of the relatively high series resistance ($6.08 \Omega \cdot \text{cm}^2$) that limits the electrical quality of the J–V characteristic. A moderate increase in electron affinity to $\chi = 4.1$ eV results in a significant improvement of the fill factor to 78.1%, mainly due to the strong reduction of the series resistance ($1.66 \Omega \cdot \text{cm}^2$). However, at $\chi = 4.2$ eV, the fill factor temporarily decreases to 72.8%, despite a relatively low R_s value ($1.51 \Omega \cdot \text{cm}^2$). This behavior can be explained by the simultaneous degradation of the shunt resistance, which drops to $179 \Omega \cdot \text{cm}^2$, indicating increased leakage currents that distort the J–V curve. In addition, the extracted ideality factor ($n \approx 1.285$) suggests the presence of moderate Shockley–Read–Hall (SRH) recombination, which may temporarily affect the junction quality.

For $\chi \geq 4.4$ eV, the fill factor increases again and eventually reaches a plateau between 81.8% and 82.0%. This improvement results from the combination of a minimal series resistance ($\approx 1.03 \Omega \cdot \text{cm}^2$) and a very large shunt resistance ($17 - 38 \text{ k}\Omega \cdot \text{cm}^2$), which significantly reduces both resistive losses and leakage currents. Despite this favorable resistive behavior, the overall device performance remains limited because the dominant recombination mechanisms at the heterointerface increase the saturation current J_0 and reduce V_{OC} [25,28]. Although fill factors above 82% indicate a very good junction quality from a purely resistive perspective, this improvement does not compensate for the large loss in open-circuit voltage. This result illustrates that in photovoltaic optimization not all parameters contribute equally to efficiency: preserving a high V_{OC} is generally more critical than maximizing the fill factor when both objectives are mutually constrained. In CIGS solar cells, the overall efficiency is therefore primarily limited by recombination processes that determine J_0 and V_{OC} , rather than by resistive effects alone [23,30].

Influence on the Power Conversion Efficiency η :-

The combined effect of the variations in J_{SC} , V_{OC} , and FF on the overall device performance is illustrated in Figure 8, which shows the evolution of the power conversion efficiency as a function of the electron affinity of the In_2S_3 buffer layer.

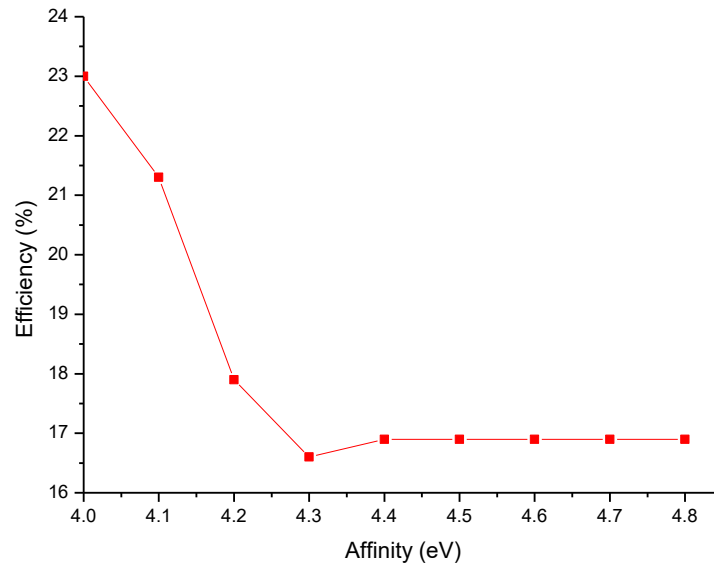


Figure 8: Efficiency profile as a function of electron affinity.

The efficiency curve clearly identifies an optimal electron affinity corresponding to the best compromise between carrier collection and recombination control, confirming the key role of the conduction band offset (CBO) in determining the performance of CIGS heterojunction solar cells [25,26]. The conversion efficiency reaches its maximum value of 22.96% for $\chi = 4.0$ eV, before rapidly decreasing to 16.6% at $\chi = 4.3$ eV, and then stabilizing around 16.9% for $\chi \geq 4.4$ eV. This three-regime behavior reflects the fundamental trade-off imposed by band alignment at the CIGS/ In_2S_3 interface, which simultaneously governs recombination processes and open-circuit voltage through the saturation current J_0 according to the Shockley relation [22,28].

At $\chi = 4.0$ eV, the positive conduction band offset ($\Delta E_c = +0.5$ eV) creates a moderate spike that effectively suppresses interfacial recombination [26]. This configuration allows the device to maintain a very high open-circuit voltage (0.988 V), even though carrier extraction is slightly limited ($J_{SC} = 32.4 \text{ mA} \cdot \text{cm}^{-2}$) and the series resistance remains relatively high. Because efficiency depends strongly on V_{OC} , the preservation of a high voltage enables the device to reach its maximum efficiency, consistent with analyses linking V_{OC} , J_0 , and radiative efficiency limits [22,28]. When χ increases from 4.0 to 4.3 eV, the conduction band offset progressively decreases, weakening the selective barrier at the interface [26,29]. Although the resulting improvement in carrier transport increases J_{SC} and reduces the series resistance, the simultaneous degradation of V_{OC} (approximately -40%) dominates the overall device behavior. Consequently, the gain in current cannot compensate for the loss in voltage, illustrating that transport optimization alone cannot offset the degradation of interfacial selectivity [24,25]. For higher electron affinity values, the cliff configuration enhances electron injection but simultaneously intensifies interfacial recombination, which increases the saturation current J_0 and severely limits the open-circuit voltage [25-27]. As a result, the efficiency stabilizes at a lower level. The narrow optimal window identified in this study ($\Delta\chi < 0.1$ eV for $\eta > 22\%$) highlights the importance of precise control over the electron affinity of the buffer layer, in agreement with previous studies emphasizing the critical role of CBO engineering in CIGS heterojunction solar cells [26–30].

Influence on the Series Resistance R_s :-

The variation of the series resistance as a function of the electron affinity of the In_2S_3 buffer layer is illustrated in Figure 9.

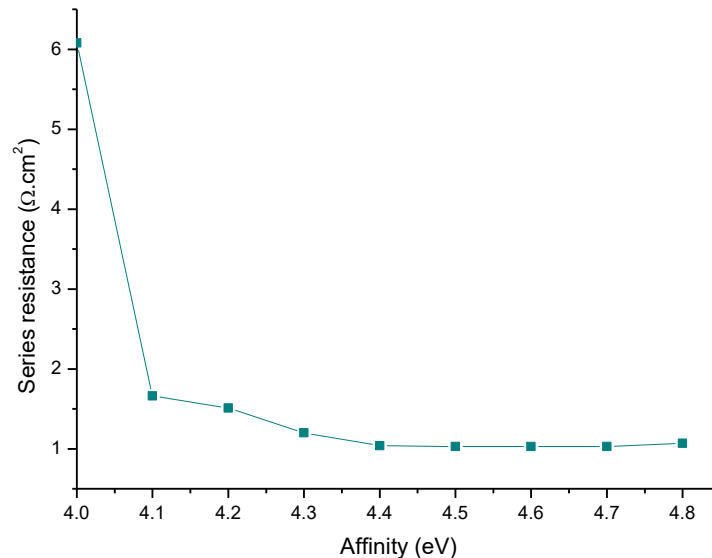


Figure 9: Series resistance as a function of electron affinity.

The results show a significant reduction in the series resistance as χ increases. This improvement represents one of the secondary beneficial effects associated with the modification of the band alignment at the CIGS/ In_2S_3 interface [25,29]. For $\chi = 4.0$ eV, the series resistance reaches $6.08 \Omega \cdot \text{cm}^2$, which strongly limits the electrical quality of the J–V curve and contributes to the relatively low fill factor observed in this configuration. When χ increases, R_s decreases rapidly, reaching values close to $1.03 \Omega \cdot \text{cm}^2$ for $\chi \geq 4.5$ eV. This evolution is consistent with improved carrier transport across the heterojunction and enhanced contact properties resulting from modifications of the band diagram [25,29]. Overall, the simulations indicate that increasing χ leads to an 83% reduction in series resistance. Nevertheless, this improvement in carrier transport does not translate into better overall device performance. Despite the significant reduction in R_s , the conversion efficiency decreases as χ increases. This behavior confirms that, in CIGS heterojunction solar cells, the dominant performance limitation is not related to resistive transport but rather to interfacial recombination mechanisms, which determine the saturation current J_0 and therefore the open-circuit voltage V_{OC} . According to the fundamental relations linking V_{OC} and J_0 , any increase in recombination strongly reduces the achievable voltage, regardless of improvements in transport properties [22,28].

Influence on the Shunt Resistance R_{sh} :-

The evolution of the shunt resistance with electron affinity is presented in Figure 10.

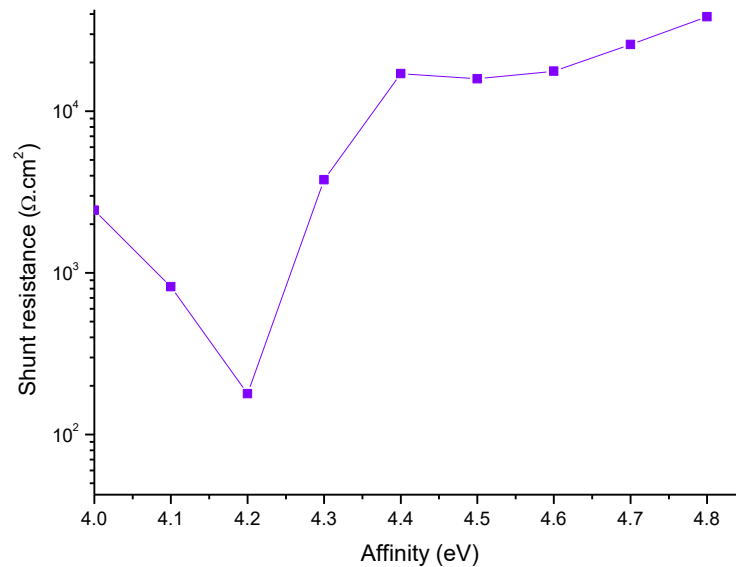


Figure 10: Shunt resistance as a function of electron affinity.

The shunt resistance generally increases with increasing χ , although noticeable fluctuations appear in the transition region around $\chi = 4.1 - 4.2$ eV. These variations are consistent with transient changes in interfacial defect states and recombination mechanisms occurring near the critical band alignment region [24,31]. For $\chi = 4.0$ eV, the shunt resistance reaches approximately $2.4 \text{ k}\Omega \cdot \text{cm}^2$, indicating the presence of moderate leakage currents. When χ increases to 4.1 eV, R_{sh} decreases to $823 \Omega \cdot \text{cm}^2$, and reaches a minimum of $179 \Omega \cdot \text{cm}^2$ at $\chi = 4.2$ eV. These fluctuations suggest temporary modifications in the junction quality or variations in the density of interfacial defect states. Beyond $\chi = 4.3$ eV, the shunt resistance increases dramatically, rising from $3.8 \text{ k}\Omega \cdot \text{cm}^2$ to nearly $38.4 \text{ k}\Omega \cdot \text{cm}^2$ at $\chi = 4.8$ eV. Such large values indicate an efficient suppression of leakage currents and reflect an excellent junction quality from an electrical perspective [25,29].

This improvement in R_{sh} contributes significantly to the high fill factor observed at large χ values. Several mechanisms may explain this behavior, including modifications in band alignment that make leakage paths energetically unfavorable, possible passivation of interfacial defects, and redistribution of the internal electric field that reduces parasitic current paths. However, despite the very high R_{sh} and improved fill factor obtained at high χ values, the conversion efficiency remains lower than that achieved for $\chi = 4.0$ eV. This confirms that the influence of shunt resistance is secondary compared with that of the open-circuit voltage, which directly depends on recombination mechanisms governed by band alignment at the heterointerface [22,28].

Summary:-

The results obtained in this simulation campaign demonstrate that the electron affinity of the In_2S_3 buffer layer plays a decisive role in determining the performance of CIGS solar cells, mainly through its control of the conduction band offset and the associated recombination processes at the heterointerface [27,29]. The optimal device performance is obtained for $\chi = 4.0$ eV, corresponding to a moderate positive conduction band offset ($\Delta E_c = +0.5$ eV) with the CIGS absorber. This spike configuration appears to be optimal despite the presence of a small energetic barrier for electron transport. Although increasing χ significantly improves several resistive parameters: such as the reduction of the series resistance, the increase in shunt resistance, and the improvement of the fill factor, these favorable effects are largely offset by the strong degradation of the open-circuit voltage. Overall, the efficiency decreases by approximately 27% between $\chi = 4.0$ eV and $\chi = 4.8$ eV, confirming that control of band alignment and suppression of interfacial recombination are the dominant factors governing the performance of CIGS/ In_2S_3 heterojunction solar cells [25–28].

Conclusion:-

This numerical study performed using the SILVACO ATLAS device simulator demonstrates that the electron affinity of the In₂S₃ buffer layer is a critical parameter controlling the performance of CIGS heterojunction solar cells. The optimal configuration is obtained for $\chi = 4.0$ eV, which yields a maximum conversion efficiency of 22.96% and an exceptionally high open-circuit voltage of 0.99 V. This operating point corresponds to a moderate positive conduction band offset ($\Delta E_c = +0.5$ eV) that effectively suppresses interfacial recombination at the CIGS/In₂S₃ interface. Although increasing the electron affinity improves carrier transport properties, leading to an 83% reduction in series resistance, a 14% increase in fill factor, and shunt resistance values exceeding $38 \text{ k}\Omega \cdot \text{cm}^2$, these improvements are accompanied by a drastic reduction in the open-circuit voltage (approximately -42%). As a result, the conversion efficiency decreases by nearly 27% between $\chi = 4.0$ and 4.8 eV. The hierarchy of the photovoltaic parameters emerging from this study is therefore clear: the open-circuit voltage plays the dominant role in determining the overall efficiency, while improvements in resistive parameters cannot compensate for increased interfacial recombination. The narrow optimal window identified in this work ($\Delta\chi < 0.1 \text{ eV}$ for $\eta > 22\%$) highlights the importance of precise control of the electron affinity through careful adjustment of material stoichiometry and deposition conditions. These results confirm the strong potential of In₂S₃ as a high-performance and environmentally friendly alternative to CdS buffer layers in CIGS solar cells. Future work should focus on experimental validation of the predicted optimal band alignment and detailed characterization of interfacial electronic properties. This study demonstrates that electron affinity engineering is a key parameter governing band alignment and interfacial recombination in CIGS/In₂S₃ solar cells. Unlike conventional approaches focusing on doping optimization, the results highlight the dominant role of V_{oc} in determining overall efficiency.

Abbreviations:-

Al: aluminum
AM1.5G: Air Mass 1.5 Global solar spectrum
CBO: Conduction Band Offset
CdS: Cadmium Sulfide
CIGS: Copper Indium Gallium Selenide (Cu(In,Ga)Se₂)
E_c: Conduction Band Minimum Energy
E_g: Optical Bandgap Energy
EQE: External Quantum Efficiency
E_{vac}: Vacuum Energy Level
E_v: Valence Band Maximum Energy
FF: Fill Factor
In₂S₃: Indium Sulfide
J_{sc}: Short-Circuit Current Density
J-V: Current–Voltage Characteristic
Mo: Molybdenum
N_A: Acceptor Concentration
N_D: Donor Concentration
η: Power Conversion Efficiency
P-V: Power–Voltage Characteristic
P_{max}: Maximum Output Power
R_s: Series Resistance
R_{sh}: Shunt Resistance
SLG: Soda-Lime Glass
SRH: Shockley–Read–Hall Recombination
TCAD: Technology Computer-Aided Design
V_m: Voltage at Maximum Power Point
V_{oc}: Open-Circuit Voltage
ZnO: Zinc Oxide
χ: Electron Affinity

References:-

1. Nakamura, M., Yamaguchi, K., Kimoto, Y., Kato, T., Sugimoto, H. et al. "Cd-Free Cu(In,Ga)(Se,S)₂ Thin-Film Solar Cell with Record Efficiency of 23.35%." Japanese Journal of Applied Physics, 2019. DOI: 10.7567/1347-4065/ab0fd6
2. Hariskos, D., Spiering, S., Powalla, M. "Buffer layers in Cu(In,Ga)Se₂ solar cells and modules." Thin Solid Films, 480–481 (2005) 99–109. <https://doi.org/10.1016/j.tsf.2004.11.118>
3. S.Spiering, A.Nowitzki, F. Kessler,M.Igalson, H.Abdel Maksoud « Optimization of buffer-window layer system for CIGS thin film devices with indium sulphide buffer by in-line evaporation » Solar Energy Materials and Solar CellsVolume 144, (2016), Pages 544-550 <https://doi.org/10.1016/j.solmat.2015.09.038>
4. Pistor, P., Caballero, R., Hariskos, D., Kaufmann, C.A. "Quality and stability of compound indium sulphide as source material for photovoltaic applications." Solar Energy Materials and Solar Cells, 93 (2009) 148–152. DOI: 10.1016/j.solmat.2008.09.015
5. B. Traoré, S. Ouédraogo, M. B. Kébré, D. Oubda, I. Sankara, A. Zongo, and F. Zougmore, "Effect of defects at the buffer layer CdS/absorber CIGS interface on CIGS solar cell performance," Advances in Chemical Engineering and Science, vol. 13, pp. 289–300, 2023. [Online]. Available: <https://www.scirp.org/journal/aces>
6. Sáez-Araoz, R., Krammer, J., Harndt, S., Köhler, T., Krüger, M., Pistor, P., Lux-Steiner, M.C., Fischer, C.-H. "ILGAR In₂S₃ buffer layers for Cd-free Cu(In,Ga)(S,Se)₂ solar cells with certified efficiencies above 16%." Progress in Photovoltaics, 2012. <https://doi.org/10.1002/pip.2268>
7. Agoundedemba, M., Baneto, M., Nyenge, R., Musila, N., Toure, K.J.N. "Improving FTO/ZnO/In₂S₃/CuInS₂/Mo solar cell efficiency using Silvaco-Atlas." International Journal of Renewable Energy Development, 12(6) (2023) 1131–1140. DOI: 10.14710/ijred.2023.57800
8. SILVACO Inc. ATLAS User's Manual / Device Simulation Software Documentation.
9. Selberherr, S. Analysis and Simulation of Semiconductor Devices. Springer, 1984. <https://link.springer.com/book/10.1007/978-3-7091-8752-4>
10. Sze, S.M., Ng, K.K. Physics of Semiconductor Devices, 3rd ed., Wiley, 2007. <https://www.semanticscholar.org/paper/Physics-of-Semiconductor-Devices%3A-Sze-Physics-Sze-Ng/281f3c1d9cc26c75c09510be27e02f11456e36e5>
11. Schroder, D.K. Semiconductor Material and Device Characterization, 3rd ed., Wiley, 2006. DOI: 10.1002/0471749095.ch2
12. W. Shockley and W. T. Read, "Statistics of the Recombinations of Holes and Electrons," Phys. Rev., vol. 87, no. 5, pp. 835–842, Sep. 1952, doi:10.1103/physrev.87.835
13. R. N. Hall, « *Electron-Hole Recombination in Germanium* », *Physical Review*, vol.87, issue.2, pp.387 387, 1952. DOI : 10.1103/PhysRev.87.387
14. Carron, R., Avancini, E., Feurer, T., Bissig, B., et al. "Refractive indices of layers and optical simulations of Cu(In,Ga)Se₂ solar cells." Science and Technology of Advanced Materials, 19(1) (2018). DOI:10.1080/14686996.2018.1458579
15. Esmaili, P., Asgary, S. "Al³⁺ Doped In₂S₃ Thin Films: Structural and Optical Characterization." Russian Journal of Inorganic Chemistry, 66(4) (2021) 621–628. DOI: 10.1134/S0036023621040094
16. Burstein, E. "Anomalous Optical Absorption Limit in InSb." Physical Review, 93 (1954) 632. <https://journals.aps.org/pr/abstract/10.1103/PhysRev.93.632>
17. Moss, T.S. "The interpretation of the properties of indium antimonide." Proceedings of the Physical Society. Section B, 67 (1954) 775. DOI:10.1088/0370-1301/67/10/306
18. Feneberg, M., Osterburg, G., et al « Band gap renormalization and Burstein-Moss effect in silicon- and germanium-doped wurtzite GaN up to 10²⁰ cm⁻³ » Physical Review B, 90 (2014) 075203DOI :10.1103/PhysRevB.90.075203
19. Rockett, A. (2010). The materials science of Cu(In,Ga)Se₂. Journal of Applied Physics, 108, 071101. <https://doi.org/10.1063/1.3489391>
20. Weinhardt, L.; Heske, C.; Umbach, E.; Niesen, T. P.; Visbeck, S.; Karg, F. "Band alignment at the i-ZnO/CdS interface in Cu(In,Ga)(S,Se)₂ thin-film solar cells." Applied Physics Letters, 84, 3175 (2004). DOI: 10.1063/1.1704877.
21. Walter, T., Herberholz, R., Müller, C., Schock, H.-W. "Determination of defect distributions from admittance measurements and application to Cu(In,Ga)Se₂ based heterojunctions." Journal of Applied Physics, 1996. DOI: 10.1063/1.363401.

22. Burgelman, M., Nollet, P., Degraeve, S. "Modelling polycrystalline semiconductor solar cells." *Thin Solid Films*, 361–362 (2000) 527–532. [https://doi.org/10.1016/S0040-6090\(99\)00825-1](https://doi.org/10.1016/S0040-6090(99)00825-1).
23. Kronik, L., Shapira, Y. "Surface photovoltage phenomena: theory, experiment, and applications" *Surface Science Reports*, 1999. [https://doi.org/10.1016/S0167-5729\(99\)00002-3](https://doi.org/10.1016/S0167-5729(99)00002-3)
24. Minemoto, T., Hashimoto, Y., Satoh, T., et al. (2001). Theoretical analysis of band alignment at CdS/Cu(In,Ga)Se₂ heterojunction. *Journal of Applied Physics*, 89(11), 8327–8330. <https://doi.org/10.1063/1.1366643>
25. Green, M. A. (1982). Solar cell fill factors: General graph and empirical expressions. *Solid-State Electronics*, 24(8), 788–789. [https://doi.org/10.1016/0038-1101\(81\)90016-6](https://doi.org/10.1016/0038-1101(81)90016-6)
26. Wei, S.-H., Zunger, A. (1998). Band offsets and optical bowings of chalcopyrites and related compounds. *Applied Physics Letters*, 72(16), 2011–2013. <https://doi.org/10.1063/1.121267>
27. Rau, U., Paetel, S., Werner, J. H. (2003). Band alignment and interface recombination in CIGS-based heterojunction solar cells. *Physical Review B*, 67, 045203. <https://doi.org/10.1103/PhysRevB.67.045203>
28. Rau, U., Schmidt, M. (2001). Electronic properties of Cu(In,Ga)Se₂ heterojunction solar cells-recent achievements, current understanding, and future challenges. *Thin Solid Films*, 387(1–2), 141–146. [https://doi.org/10.1016/S0040-6090\(00\)01871-4](https://doi.org/10.1016/S0040-6090(00)01871-4)
29. Shockley, W. (1949). The theory of p–n junctions in semiconductors and p–n junction transistors. *Bell System Technical Journal*, 28(3), 435–489. <https://doi.org/10.1002/j.1538-7305.1949.tb03645.x>
30. Gloeckler, M., Sites, J. R. (2005). Band-gap grading in Cu(In,Ga)Se₂ solar cells. *Journal of Physics and Chemistry of Solids*, 66(11), 1891–1894. <https://doi.org/10.1016/j.jpcs.2005.07.024>
31. Jackson, P., Wuerz, R., Hariskos, D., et al. "Effects of heavy alkali elements in Cu(In,Ga)Se₂ solar cells ..."
Physica Status Solidi RRL, 2016. DOI :10.1002/pssr.201600199